Accepted Manuscript

Title: Comparison of ballistic performances of Al_2O_3 and AlN ceramics

Author: M. J.Pawar, A. Patnaik, S.K. Biswas, U. Pandel, I.K. Bhat, S. Chatterjee, A.K. Mukhopadhyay, R. Banerjee, B.P. Babu

PII: S0734-743X(16)30504-8
DOI: http://dx.doi.org/doi: 10.1016/j.ijimpeng.2016.08.002
Reference: IE 2729

To appear in: *International Journal of Impact Engineering*

Received date: 4-12-2015
Revised date: 4-7-2016
Accepted date: 3-8-2016

Please cite this article as: M. J.Pawar, A. Patnaik, S.K. Biswas, U. Pandel, I.K. Bhat, S. Chatterjee, A.K. Mukhopadhyay, R. Banerjee, B.P. Babu, Comparison of ballistic performances of Al_2O_3 and AlN ceramics, *International Journal of Impact Engineering* (2016), http://dx.doi.org/doi: 10.1016/j.ijimpeng.2016.08.002.

Comparison of Ballistic Performances of Al_2O_3 and AlN ceramics

M. J.Pawar[1], A.Patnaik[1], S.K.Biswas[1♣], U.Pandel[1], I. K.Bhat[1], S.Chatterjee[2], A. K.Mukhopadhyay[2], R.Banerjee[2], B.P.Babu[3],

[1]Malaviya National Institute of Technology, Jaipur-302017, India

[2]CSIR- Central Glass & Ceramic Research Institute, Kolkata-700032,India

[3]Ordnance Development Centre, Ordnance Factory Medak, Telangana-502205, India

Highlights

- Ballistic Performances of AlN/Al5083 and Al_2O_3/Al5083 armor configurations have been compared.
- Backing Plate Deformation of AlN/Al5083 is much less than that of Al_2O_3/Al5083 armor
- Finite Element simulation has been validated with experiment.
- Higher performance of AlN is due to higher shear strength and Hugoniot Elastic Limit of AlN than that of Al_2O_3.

♣ Corresponding author: sbiswas.meta@mnit.ac.in, FAX no.00912412529029

Graphical Abstract

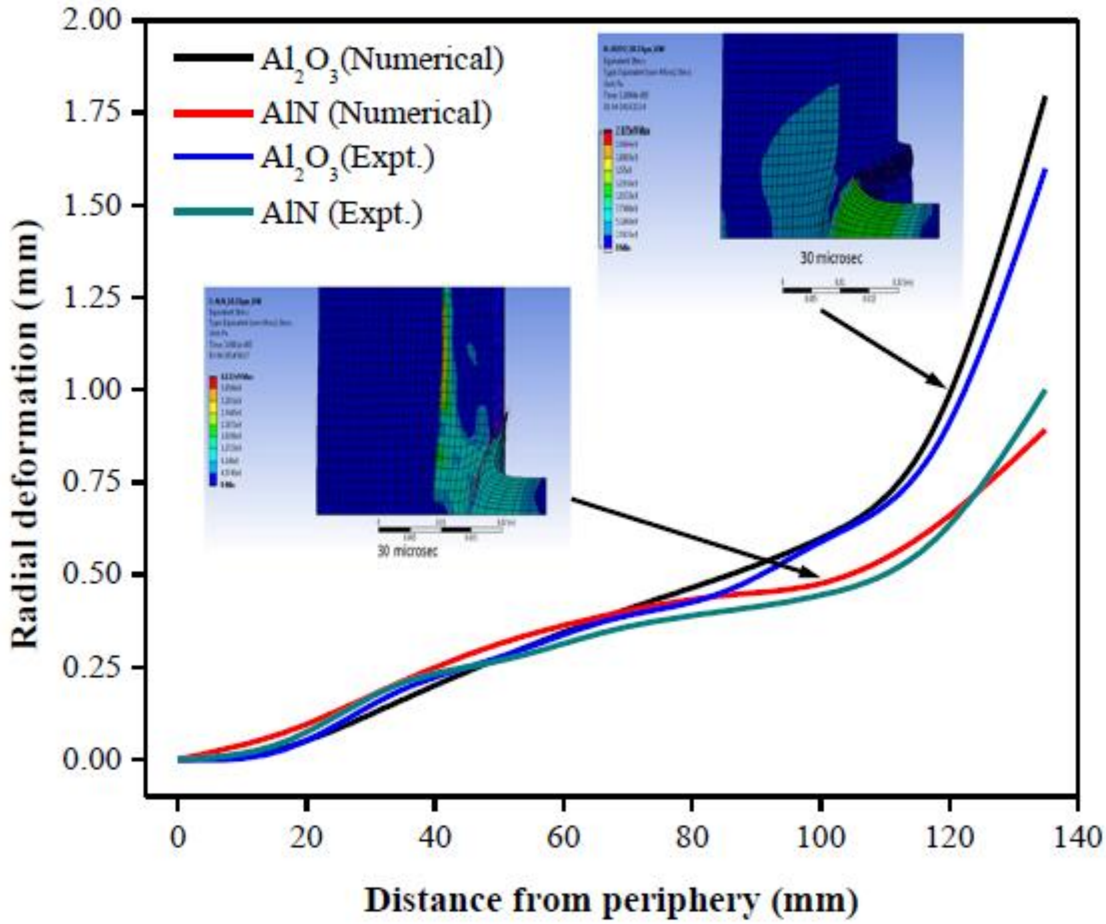

ABSTRACT

Finite Element Analysis of the impact of 7.62AP Bullets on Ceramic/Aluminum bi-layer hybrids were carried out using AUTODYN hydrocode. Johnson-Cook material model was used for the metal and Johnson-Holmquist model was used for the ceramic. The models were validated with experiments conducted on Al_2O_3/Al 5083 and AlN/Al 5083 bi-layer composites. It has been observed that AlN ceramics has superior performance in defeating the bullet in comparison to Al_2O_3 ceramics. Deformation of the backing plate and the corresponding plastic strain energies are considered in this study for the parameters of performance. The results will enable the design

of materials for developing an efficient structure for the protection against the impact of 7.62AP bullets at ordnance velocities.

Keywords: Al_2O_3; AlN; Al 5083; Armor; Ballistic Impact

1. Introduction

Over the last five decades significant researches have been carried out to understand the failure mechanisms of the composite panels. Florence [1] studied the impact of 0.30Cal and 0.45Cal bullets on Al_2O_3 and B_4C tiles of different thicknesses. Wilkins [2] studied the penetration and perforation characteristics of the alumina/aluminum composite target using surrogate armor piercing bullets of diameter 7.62 mm. Formation of cone crack in ceramics and subsequent dissipation of the energy of the projectile to deform the metallic backing plate is the main mechanism for the absorption of kinetic energy of the projectile by the metal/ceramic composite target [1-5]. Failure in the ceramic plate initiates from the ceramic/metal or more precisely ceramic/adhesive interface at the rear end of the ceramic tile [1,2,6]. Compressive stress pulses generated by the contact of the projectile on the ceramic surface travel through the thickness of the ceramic tile and a major portion of it reflected back from the backing material which has usually lower impedance than the ceramics. The mode of the stress waves becomes tensile while traveling in the opposite direction and cause the generation of cone crack from the projectile/ceramic contact end and proceeding towards the tile/support interface where the base of the conoid is formed [1,7-9]. Controlled experiments carried out in Split Hopkinson Pressure Bar (SHPB) by terminating the axial loading at different times and analyzing the axial sections show that the base of the conoid develops first from the opposite face of the ceramic sample from the striking end [10,11]. Analyses revealed that the development of the conical damage zone takes time to reach the contact surface of the projectile known as "Dwell" after which the fragmented or deformed projectile starts to penetrate the ceramics[6,12-14]. The ceramic conoid effectively distributes the incident force over a larger area on the backing plate. Radial cracks are also formed during the impact [1,7-9,15-17]. Conoid apex angles have been observed to be 66^{o}[1]which varies with the chemical composition of the ceramics and impact velocity of the projectile [18].

The pressure from the ceramic conoid base deforms the backing plate which absorbs the remaining kinetic energy of the bullet fragment. The change in kinetic energy of the bullet depends on the impact velocity or more precisely impact energy for a fixed material parameter like chemical composition and thickness of the tile and the backing layer. The change is maximum when the bullet is stopped by the target at the limit velocity. Further increase of the velocity makes the target perforated by the bullet and the energy change becomes less than that of ballistic limit velocity [19]. Deformation of the backing plate is, therefore, a measure of the efficiency of a ceramic/metal hybrid panel. Less deformation indicates larger absorption of the energy of the projectile in interaction with the ceramic tile. Moreover, design of ceramic composite armor involves lay out plan of mosaic arrangement of tiles. In mosaic tile arrangement too much bulging or radial deformation of the backing plate can cause detachment of the neighboring tiles from the backing plate and make the composite structure more vulnerable to multiple hits of bullets. Optimization of the back-face deformation in the hybrid structure is, therefore, necessary to evolve an efficient protection mechanism for the armor designers.

While determining the performance of different ceramics in plate impact and SHPB experiments and validating the corresponding damage model [20-28] it could be observed that the failure mechanisms of different ceramics are very complex and different. Complication increases with the phase change and brittle to ductile transitions of certain materials at different levels of stresses[10, 26]. Very few experiments have been known [21,29-31]to compare the dynamic properties and performances of different ceramics under similar impact conditions. Most of the studies concentrated on determining the performance parameter of the ceramics in terms of mass and thickness efficiencies and ballistic limit velocities or depth of penetrations.

The objective of the present study is, therefore, to find out the performance of two different ceramic materials arising out of their constitutive properties apart from mass efficiencies when adhered in front of a metal plate of similar chemical composition, heat treatment condition and thickness. The choice of Al_2O_3 and AlN has been made due to the available information in the literature on the dynamic behavior of these materials at high strain rates[3, 6, 10, 25, 28, 32, 33].Stress has been put, in this study, on the comparison of the backing plate (Al-5083 wrought alloy) deformation and the energy associated with it assuming maximum absorption of kinetic energy of the bullet by the test panel [19].Deformation of the backing plate (Al-alloy) having finite thickness (20mm)after striking with the bullets with ceramic plates adhered to the striking surface were first determined by numerical simulation using AUTODYN3D hydrocode and then validated through experiments. 7.62 AP round and an instrumented standard Dragunov Rifle (B32,USSR) were used to launch the projectile at a distance of 10Meter from the target.

2. Experimental Method

AlN tiles have been prepared in-house by pressure-less sintering of AlN powder with Y_2O_3 sintering additive. Al_2O_3 ceramics and Al 5083 wrought alloy have been procured commercially. In present study the 99% pure Al_2O_3 with density of 3.82g/cc is used.Al_2O_3 tiles were produced by pressure less sintering with $CaSiO_3$ additive. The specifications of the bullet, backing plate and the ceramic tiles are presented in Table 1 and 2 respectively. Wrought Al-5083 alloy blocks and plates of diameter 270 mm and thickness t (t=125mm, 60mm and 20mm) were used with both the faces machined and ground. Single ceramic tiles (50mm × 50mm × 8mm) were bonded at the center of the circular surface of the metal blocks/plates with a polyurethane adhesive to fabricate each ceramic/metal hybrid test panel (Fig.1). The thickness of the adhesive was maintained constant (0.5mm) in each configuration. The tiles were covered with glass fiber cloth to minimize the loss of debris by spallation during the impact with the bullets without imposing any constraint to the tiles. A GFRP frame (150mm × 150mm × 10mm) was also used to minimize the flying of ceramic tile pieces after being hit by the bullet (Fig. 1). However, care was taken so that the ceramics are not under any confinement by the GFRP guard. The periphery of the backing plate was rigidly clamped in a steel frame with the help of C-clamps and other bolted fixtures and placed at a distance of 10Meter from the launching end of a fixed Dragunov Rifle.

Normal incidence of the bullet on the target surface during the impact has been ensured in a standard test range. Velocities of the bullets were measured by the time of travel of the bullets between two light screening gauges placed parallel at a fixed distance. Three tests were performed for each ceramic/metal target configuration and the average values were taken for the analysis of results.

Depth of reference penetration (DOP) in the semi-infinite Al-5083 blocks hit by the bullets was measured after machining the block from the opposite surface till the tip of the bullet was observed. Since there was no penetration of the bullet except a crater, formed behind the ceramic/metal interface on the backing plate surface when ceramics were used, the depth of the crater was measured from the ceramic/metal interface. Deformation (bulging) of the backing plate (D) of thickness 20mm was measured by means of a surface planometer. Radiographic images of the ceramic tiles were checked for the presence of any macroscopic defect before fixing on the backing plates.

Scanning electron microscope (SEM) examination of the fracture surfaces of the samples were carried out using a ZEISS SUPRA 35 VP FESEM. Transmission electron microscope (TEM) (Tecnai G2 F30 ST 300kV, FEI) was used to observe the thin foils of ceramics after thinning down of the specimens by dimpling and ion beam thinning.

3. Numerical Simulation

Lagrangian approach is used to develop numerical model for simulation of high velocity impact carried out to assess the impact resistance of a composite panel with front faced ceramic plate and ductile aluminum alloy back plate. The details of the target, projectile and the support conditions are provided in following sub-sections.

3.1 Geometry and finite element discretization:

Three dimensional finite element meshes of the target panel and projectile used in finite element model is shown in Fig. 2. The minimum size of the element used is 0.25 mm. Number of eight noded brick finite elements for the projectile geometry and target bodies are about 1920 and 123472, respectively. After various trials on mesh size the final target discretized with uniform refined mesh as shown in Fig. 2 is used. To minimize the time required for computation the analysis is made on quarter model of entire geometry as shown in Fig. 3a. Although the actual configuration of the bullet comprises of a thin casing and inner core, but ogive nosed monolithic projectile is used for the simulation to save computational time as the observation made earlier [34] that stripping of the bullet casing consumes very little kinetic energy of the bullet during penetration. Care is taken to keep the momentum and kinetic energy of the projectile same as those used during the impact tests. The output parameters like projectile velocity, depth of penetration, back face and radial deformations are measured at respective points as shown in Fig. 3b.

3.2 Interface model:

Modeling of interface has importance on ballistic performance of layered structure [35, 36]. Representation of interfaces needs keen attention when constructing finite element models for performance assessment of layered structures. Interfaces may be modeled according to one of two conditions: (i) tied bonding, corresponding to shared nodes and perfect coherence or (ii) free contact, corresponding to duplicate nodes along distinct, interacting frictionless surfaces [35]. In present study front ceramic tile and ductile back plate of target are bonded with the polyurethane resin. The interfaces (ceramic tile -polyurethane adhesive and polyurethane adhesive -Al-5083back plate) are modeled as bonded contact region between surface to surface subjected to failure at 1.5 times geometric strain limit. The contact between the GFRP and back plate is also modeled as bonded contact. The contact is not generated between projectile and ceramic.

3.3 Boundary conditions

Curved surface of metallic back plate is constrained to move in any direction using fixed support. The velocity of projectile at the instant of first contact with the target is 840 m/s whichreduce with the dissipation of kinetic energy during the penetration. Hence, the finite element model of projectile is provided with initial velocity of 840m/s.

3.4 Material models

Table 3 provides the compilation of material models used in the study. It is very important to use improved material models and their input data when modeling any material under shock loads to obtain better results. Three important descriptors are needed for representing material behavior under high velocity impact as given below:

- An equation of state (EOS) which relates the density (or volume) and internal energy (or temperature) of the material to pressure.
- A constitutive relationship which describes the strength of the material by relating the stress in the material to the amount of distortion (strain) required to produce this stress.
- A failure model to predict the failure of material.

The behavior of the polyurethane adhesive is considered as visco-elastic, on the basis of the variation of the elastic modulus with the strain rate. In presence of shock EOS the tension waves reaching the ceramic–adhesive interface are visco-elastic [37]. When Lagrangian scheme is used for simulation, numerical difficulties arising from excessive distortion of element mesh are often overcome by using an erosion criterion. Lagrangian system is used to allow unstable or highly distorted elements to be deleted or eroded [38].Hence, in addition to the above requirements, an erosion criterion is also required as an effective numerical tool to handle severe mesh distortion in both projectiles and target. However, it needs careful tuning of the correct values of geometric strains for the material so that numerical computation does not get interrupted. It is observed from the literature that different values of the geometric erosion strains may be possible for same materials because it is not a material property, but a numerical technique to remove severely distorted elements from computation.

3.4.1 Material models for various constituents of armor panel and projectile

Johnson-Holmquist (JH-2) model is one of the most widely used models for the study of ceramics under ballistic impact. The inelastic behavior of brittle material (like ceramic) whose strength is affected due to crushing is suitably represented in the JH-2 constitutive model [39]. The strength parameters like yield, shear modulus are reduced with the progression of damage.JH-2 Model for both strength and damage modeling in the ceramic tiles is used in the present study for ceramic plates in the simulations. The model consists of three parts, namely strength, damage and pressure models. JH-2 material strength and damage models are smooth analytical functions of pressure. The strength in terms of von Mises equivalent stress (σ) is represented by the expression,

$$\sigma_0 = \sigma_i + (\sigma_{max} - \sigma_i)\{1\text{-exp-}\alpha_i(P\text{-}P_i)\} \quad (1)$$

where, $\alpha_i = \sigma_i/[(\sigma_{max} - \sigma_i)(P_i + T)]$.

Strength (σ) increases linearly from the hydrostatic tensile failure limit (-T) to the strength of the intact material (σ_i). Similar expression could be stated for the strength of the failed material which takes a linear increase from 0 at P=0 to σ_f at P=P_f. Thus,

$$\sigma_{0f} = \sigma_f + (\sigma_f^{max} - \sigma_f)\{1\text{-exp-}\alpha_f(P\text{-}P_f)\} \quad (2)$$

where, $\alpha_f = \sigma_f/[(\sigma_f^{max} - \sigma_f)(P\text{-}P_f)]$.

Eqs. (1) and (2) are for dimensionless strain rate, ε^* =1. The strengths at different strain rates could be obtained from the relation,$\sigma = \sigma_0(1\text{+Cln } \varepsilon^*)$ where C is a dimensionless constant.

In JH-2 models, the failure affects the strength of the intact material differently. JH-2 model allows for the gradual softening of the material as the damage progresses from 0(intact) to 1(fully damaged). JH-2 models are used in conjunction with polynomial equation of state when bulking constant is greater than zero. The model has been used to allow for principal tensile failure initiation in addition to the hydrodynamic tensile limit. The crack softening algorithm can also be used in conjunction with principal stress failure criteria.

The strength of projectile (Steel grade 4340)and metallic back plate (Al5083H116)is modeled using Johnson-Cook (JC)strength and failure model[40, 41]. The model was developed to describe a phenomenological deformation for metals with respect to strain, strain rate and temperature[40].The flow stress (von Mises) in JC model is expressed in terms of an explicit function of strain hardening, strain rate hardening and thermal softening phenomena. The governing equation can be described below.

$$\sigma = [A' + B' (\varepsilon_p)^n] [1+C'\ln (\dot{\varepsilon}/\dot{\varepsilon}_0)][1- [(T- T_0)/(T_m-T_0)]^m] \quad (3)$$

where, A' is the initial yield stress, B' is the strain hardening coefficient, 'ε_p' is the effective plastic strain, 'n'is the strain hardening exponent, $(\dot{\varepsilon}/\dot{\varepsilon}_0)$ is the normalized strain rate in which $\dot{\varepsilon}$ is the effective plastic strain rate and $\dot{\varepsilon}_0$ is the reference strain rate, C' is the strain rate coefficient, 'm' is the temperature softening exponent, $(T- T_0)/(T_m-T_0)$ is the normalized temperature in which T, T_0 and T_m are temperature, room temperature and melting temperature, respectively.

The failure of projectile is defined by the failure model [41]. The metallic back plate is subjected to hydrostatic pressure and gets deformed. Hence, failure of metallic back plate is defined by minimum hydro pressure. Whereas, JC model is used in conjunction with linear equation of state for the deformation of the projectile and metallic back plate. The adhesive (polyurethane) is modeled with the help of only shock equation of state. Initially, the experimental ballistic limit velocity [42] was tested by simulation with AUTODYN3D hydrocode. The model was validated with the experimental results described below in the present investigation.

4. Results and Discussions

4.1 Experiments

Fig. 4 shows the SEM microstructures of the fracture surface of the two ceramic materials generated under quasi-static load. Average grain sizes are smaller in AlN than in Al_2O_3 samples. A little glassy phase could be observed in Al_2O_3 samples. Mostly intergranular fracture took place in Al_2O_3 samples while in AlN samples mostly the fracture is mixed mode in nature. Many trans-granular cleavage steps could be visible in AlN samples.

Fig. 5(a) shows projectile penetration on the semi- infinite Al 5083-alloy (without ceramics) block (125mm thickness and 270mm dia). Fig. 5(b) shows the tip of the bullet embedded in the metal. The DOP was found to be 62.5 mm (Average of three values). It was evident that ductile hole enlargement due to high radial pressure during the passage of the projectile [42] has taken place. Distinct bulging in the periphery on the hole entrance had been observed (Fig. 5a). Fig. 5c and 5d show the damage of the ceramic front plates after the impact with 7.62AP bullets for Al_2O_3 and AlN ceramics respectively.

4.1.1 Deformation of backing plate and strain energy:

The deformation of the backing plate could be described in Fig. 6 considering isotropic circular membrane loaded at center and clamped around edges. The deformation (ω) could be represented by [43],

$$\omega = p/16\pi D\,[(\alpha^2 - r^2) + 2r^2 \log (r/\alpha)] \qquad (4)$$

where, p- load at the center, $D = Eh^3/12(1-\nu^2)$, h – thickness of the plate (20mm), ω_0 – maximum deformation and α - radius of the membrane (135mm).

Strain Energy for the deformation is represented by,

$$W = \frac{D}{2}\int_0^{2\pi}\int_0^{\alpha}\left(\frac{\delta^2\omega}{\delta r^2} + \frac{1}{r}\frac{\delta\omega}{\delta r}\right)^2 r dr d\theta \qquad (5)$$

and the maximum plate deflection

$$\omega_0 = p\alpha^2/16\pi D \qquad (6)$$

Integrating the right hand side of Eq. (5) by parts gives the strain energy,

$$W = 55.9\pi D\omega_0^2/\alpha^2 \qquad (7)$$

Introduction of the mechanical properties and dimensions (E=71GPa, h=20mm, ν=0.3, α= 135mm) of the backing plate (Table 2 and Figs.6 and 7) and the average maximum plate deflection (ω_0 – 1.5mm when Al_2O_3 and 1mm when AlN tiles were used) in Eq. (7) produces strain energy values (W) 1.026kJ when Al_2O_3 and 0.455kJ when AlN tiles were used on the striking face. The value of the strain energy is almost 27% of the kinetic energy of the bullet (3.729kJ) for Al_2O_3 tiles and 12.22% for AlN tiles. Similar distribution of residual strain energy after the impact with 7.62AP bullet on Al_2O_3/GFRP target has been obtained by earlier studies [44]. However, no literature data could be obtained on the deformation of backing plate for the AlN/Al-alloy bilayer composite. Thus, the deformation profile and the strain energy of the backing plate could be determined fairly on the basis of the assumption of maximum energy absorption in the just stopped condition of the projectile and isotropic elastic properties of the membrane. Measured depth of penetration and back-face deformation values are presented in Table 4.

4.2. Computational Model

Fig. 8 shows the comparison of the penetration histories of projectiles in Al_2O_3/Al5083 and AlN/Al5083armor plates striking at 840 m/s. The frames are at an interval of 10 microseconds. Within 30 microseconds the bullet has penetrated the Al_2O_3tile. From 30 microseconds onward the remaining kinetic energy of the bullet mass is absorbed by Al5083 back plate which results in the deformation of the back plate in the form of bulging.Al_2O_3 tiles damaged rapidly in a brittle manner showing marginal flattening of the front tip of the bullet penetrating inside the armor plate more deep in comparison to AlN ceramic. In case of Al_2O_3/Al5083 armor plate the bullet is arrested after complete damage of the ceramic tile and partial damage of back plate. The bullet is not able to penetrate the AlN tile completely and maximum amount of kinetic energy of the bullet is dissipated to damage AlN facing material which shows higher resistance to penetration. It is interesting to note that AlN tile resists and causes more damage to the bullet thus reducing the length of the bullet. The tip of the bullet is flattened and mushroomed and the remaining kinetic energy of the bullet mass and the advancing ceramic cone is absorbed by the backing plate which is marginal. Erosion of the bullet is rapid and higher in AlN tiles than in Al_2O_3 tiles. Fig. 9 shows the damage propagation in the Al_2O_3 and AlN ceramic tiles respectively. The intensity of damage in Al_2O_3 is more. The bullet comes to rest after 44 microseconds and 60 microseconds for armor plate with AlN and Al_2O_3 facing materials respectively (Fig. 10). Evolution of back face deformations for the armor plates with time are shown in Fig.11. It could be observed that the total deformation for Al_2O_3/Al5083 armor plate is much higher (1.79mm) than that for AlN/Al5083 armor plate (0.84mm). Moreover, increase of deformation in case of Al_2O_3/Al5083 armor plate after 30 microseconds is due to the impact of remaining portion of the bullet on the backing plate (Fig. 8) as a result of complete pulverization of the ceramic in front of the deformed projectile. Whereas, for AlN/Al5083 armor after 30 microseconds the tip of the bullet got blunted and mushroomed when most of the kinetic energy of it is dissipated and further penetration is resisted. The histories of the depth of penetration of projectiles in two armor plates are shown in Fig. 12. Total penetration depth is 6.5 mm for Al_2O_3 faced armor and 1.89mm for AlN faced armor. The simulation results closely match with the experimental results (6.4mm for Al_2O_3 and 2.5mm for AlN). Fig. 13 shows the comparison of radial deformation of the backing plates for the two ceramics Al_2O_3 and AlN placed at the striking front of the target test plates. It could be observed that the experimentally observed deformation of the backing plates are almost similar to those arrived with the simulation studies. Slight lower experimental deformation values in case of Al_2O_3 and higher in case of AlN than those observed from simulations are due to the incorporation of library values of the AUTODYN software in the simulations.

Lower strain energy in the backing plates when AlN tile was used implies greater efficiency of AlN material over Al_2O_3 in reducing the kinetic energy of the bullet. The reason may be the higher Hugoniot Elastic Limit (HEL) value of AlN (9.4GPa) [45] and shear strength than those of Al_2O_3 (6-7.5GPa)[46]. However, earlier studies showed that HEL values of ceramics do not have strong correlation with their ballistic performances [31,47]. Compressive strength of pressureless sintered AlN increases to 4.5GPa at a strain rate of $10^3 s^{-1}$[10]. Fracture mechanism of AlN changes from the quasi-static to dynamic loading conditions [32]. Shear strength of ceramics plays a greater role in damage initiation during dynamic loading [31,47]. Nucleation and growth of tensile cracks at grain boundaries or hetero-interfaces cause the generation of wing cracks as a result of shear displacement of grain boundaries [48-50]. Micro-plasticity of the material controls the shear failure by accommodating the shear stresses and suppressing the wing cracks. Under dynamic loading condition the suppression in wing crack formation should delay the damage or failure of the material. A non-dimensional ductility parameter (Δ^*) was introduced to account for the suppression of nucleation and growth of wing cracks in brittle materials [48].

$$\Delta^*=(K_{IC}/\delta c)/(\sigma_y/2) \quad (8)$$

where 'K_{IC}' is fracture toughness of ceramics having a critical crack size '2c' and 'σ_y' is the yield stress.

Shear strength of Al_2O_3 reaches 2.75GPa above its HEL while that of AlN reaches 3.5 GPa above the HEL and increases further with the applied shock stress over 16 GPa [45, 46]. Thus, primarily, the Yield strength controlled the ductility of the two ceramics (Al_2O_3 and AlN) studied in the present investigation since K_{IC} values of the two materials do not differ much. It has been observed earlier that substantial amount of dislocation and consequent permanent strain and stored energy develop in AlN ceramics during the impact of bullet (7.62 NATO round) on ceramic tiles not supported by backing plate [51]. Nevertheless, dislocations could generate in both AlN and Al_2O_3 under the ballistic impact conditions [28,32,51,53]. Higher plasticity of AlN in comparison to that of Al_2O_3 indicated by the lower hardness of AlN than that of Al_2O_3 at room temperature should exhibit higher dislocation density and consequently the stored energy in the former material. Al_2O_3 exhibits microplasticity at a much higher confinement stress in comparison to AlN [10,28,54,55]. It had been observed that a Vicker's indentation load could initiate Basal and Prismatic glide with slip systems (0001) <1120> and {1100}<1120> in AlN [56]. Moreover, AlN exhibits phase transition from wurtzite to rock salt structure at a pressure of 20GPa, usually encountered by the ceramics during bullet impact [57]. Such phase transition is not exhibited by Al_2O_3. AlN tiles due to the phase transition and higher microplasticity should dissipate much greater amount of bullet energy than Al_2O_3 tiles which do not undergo any phase transition. TEM images of the specimens of AlN samples both before and after the impact in the present study are presented in Fig. 14. Fig. 14(a) shows the presence of very few defects like stacking faults and dislocations near the boundaries of a few grains. These defects arise due to the thermal history in processing of the samples. However, Fig. 14(b) representing the TEM image of a recovered sample after the bullet impact shows a huge increase in the densities of dislocations and the interaction of them with the strain contours. Detailed analysis of the dislocations and their role in failure of the two ceramics is being carried out and will be communicated for publication shortly. Recently, two different types of deformation mechanisms have been demarcated in pressure sensitive (low pressure) and insensitive (high pressure) regions [32,52].The authors have hypothesized that a flaw controlled failure in the lower pressure region below the transition to inelasticity is essentially governed by the existing flaws creating "wing cracks". Above the brittle to ductile transition pressure suppression of wing crack and a dislocation controlled failure mechanism is, therefore, assigned to the damage mechanism of AlN in the present study.

5. Conclusions

The present study has shown that deformation of the backing plate in a ceramic/Al-5083 bi-layer composite is dependent on the chemical composition of the ceramic material. AlN is superior to Al_2O_3 in creating less bulging of the backing plate. Plastic strain energy of the backing plate is much less when AlN constitutes the front layer of the composite indicating its superior performance to Al_2O_3. Higher shear strength of AlN over that of Al_2O_3 governing the suppression of wing crack formation under compressive load has been proposed to be the main reason making AlN more efficient than Al_2O_3.

Acknowledgement

Council of Scientific and Industrial Research (CSIR) network project no. NWP-0029 for sponsorship and Material Research Center (MRC), MNIT, Jaipur for the support in TEM examination of samples.

References

[1] A. L. Florence, Interaction of projectiles and Composite armor. COMPOSITE PART 11,Stanford Research Institute, Report No.AMMRC-CR-69-15, USA, 1969.

[2] M. L. Wilkins, Mechanics of penetration and perforation, Int J Eng Sci, 16(11) (1978) 793–807.

[3] D. A. Shockey, A.H. Marchand, S.R. Skaggs, G.E. Cort, M.W. Burkett, R. Parker, Failure phenomenology of confined ceramic targets and impacting rods, Int J Impact Eng 9 (1990)263-275.

[4] D. A. Shockey ,D.J. Rowliff , K.C. Dao L. Seaman, Particle Impact Damage in Silicon Nitride, J Am Ceram Soc73 (1990)1613-1619.

[5] D.R. Curran, L. Seaman, T. Cooper, D. A. Shockey, Micromechanical model for comminution and granular flow of brittle material under high strain rate application to penetration of ceramic targets, Int J Impact Eng 13 (1993) 53-58.

[6] T. J. Holmquist, D. W. Templeton, K. D. Bishnoi, Constitutive Modeling of Aluminum Nitride for Large Strain, High-Strain Rate, and High-pressure Applications, Int J Impact Eng 25(2001) 211-231.

[7] D. Sherman, Impact failure mechanisms in Alumina tiles on finite thickness support and the effect of confinement, Int J Impact Eng 24 (2000) 313-328.

[8] D. Sherman, T. Ben-Shushan, Quasi-static impact damage in confined ceramic tiles, Int. J Impact Eng 21 (1998) 245-265.

[9] R. Zaera, V. Sanchez-Galvez,Analytical modelling of normal and oblique ballistic impact on ceramic/metal lightweight armours, Int J Impact Eng 21(1998)133-148.

[10] W. Chen, R. Ravichandran, Static and Dynamic Compressive behavior of Aluminum Nitride under moderate confinement, J Am Ceram Soc 79(1996)579-584.

[11] W. Chen, R. Ravichandran, Dynamic compressive failure of glass ceramic under lateral confinement, J. Mech. Phys. Solids 45(1997)1303-1328.

[12] P. Lundberg, R. Renstrom, L. Holmberg, An experimental investigation of interface defeat at extended interaction time, in: Proceedings of the 19th International Symposium on Ballistics, 3 (2001) 1463–1469.

[13] L. Westerling, P. Lundberg, B. Lundberg, Tungsten long rod penetration into confined cylinders of boron carbide at and above ordnance velocities, Int J Impact Eng 25(2001)703-714.

[14] P. Lundberg, R. Renstrom, B. Lundberg, Impact of metallic projectile on ceramic targets: transition between interface defeat and penetration, Int J Impact Eng24 (2000)259-275.

[15] D. Sherman, D.G. Brandon, The ballistic failure mechanisms and sequence in semi-infinite supported alumina tiles,J Mater Res12 (1997)1135-1343.

[16] I. Horsfall, D. Buckley, The effect of through-thickness cracks on the ballistic performance of ceramic armour systems, Int J Impact Eng 18(1996)309-318.

[17] C. Navarro, M.A. Martinez, R. Cortes, V. Sanchez-Galvez, Some observations on the normal impact on ceramic faced armors backed by composite plates, Int J Impact Eng 13(1993) 145-156.

[18] J.E.Field, Q.Sun, D.Townsend, Ballistic impact of ceramics, in Proc. of the fourth international conference on the mechanical properties of materials at high rates of strain, Oxford, 19-22 March, 1989, IOP publishing Ltd., England.

[19] J.G. Hetherington, B.P. Rajagopalan, Energy and momentum changes during ballistic perforation, Int J Impact Eng 18(1996) 319-337.

[20] N.K. Bourne, On the failure and dynamic performance of materials, Exp Mech 52(2012)153-159.

[21] D. E. Grady, Shock-wave compression of brittle solids, Mech Mat 29(1998)181-203.

[22] W. W.Chen, A.M. Rajendran, B. Song, X. Nie, Dynamic fracture of ceramics in armor applications, J Am Ceram Soc 90 (2007)1005-1018.

[23] W. Chen, G. Ravichandran, Failure mode transition in ceramics under dynamic multiaxial compression, Int J Fracture 101(2000)141-159.

[24] G.Subhash, G. Ravichandran, Mechanical behavior of a hot pressed aluminum nitride under uniaxial compression, J Mater Sci 33 (1998) 1933-1939.

[25] G.R Johnson, T. J Holmquist, S.R. Beissel, Response of Aluminum Nitride (including a phase change) to large strain, high strain rates and high pressure, J Appl Phys 94(2003)1639-1645.

[26] T.J. Holmquist, G.R. Johnson, Characterization and evaluation of Boron Carbide for plate impact conditions, J Appl Phys100(2006) 0935251-13.

[27] Z. Rosenberg, Y. Yeshurun, The relationship between ballistic efficiency and compressive strength of ceramic tile, Int J Impact Eng 7(1988)357-362.

[28] J. Lankford, W. W. Predebon, J. M. Staehler, G. Subhash, B. J. Pletka, C. E. Anderson, The role of plasticity as a limiting factor in the compressive failure of high strength ceramics Mech Mater29(1998)205-218.

[29] J.E. Reaugh, A. C. Holt, M.L. Wilkins, B. J. Cunningham, B. L. Hord, A. S. Kusubov, Impact studies of five different ceramic materials and pyrex, Int J Impact Eng 23(1999)771-782.

[30] R.R. Franzen, D.L. Orphal, C. E. Anderson Jr., The influence of experimental designon Depth-of penetration (DOP) test results and derived ballistic efficiencies, Int J Impact Eng 19(1997) 727-737.

[31] N. K. Bourne, The relation of failure of 1D shock to the ballistic performance of brittle materials, Int J Impact Eng 35(2008) 674-683.

[32] G. Hu, C.Q. Chen, K.T. Ramesh, J.W. McCauley, Mechanisms of dynamic deformation and dynamic failure in aluminum nitride, Acta Mater 60(2012)3480-3490.

[33] N.K.Bourne, Impact of Alumina I, Response at mesoscale, Proc R Soc A, 462(2006) 3061-3080.

[34] P. J. Hazell, Measuring the strength of brittle materials by depth-of-penetration testing, Adv Appl Ceram 109(2010) 504-510.

[35] J. D. Clayton, Modeling and Simulation of Ballistic Penetration of Ceramic Polymer Metal Layered Systems, Mathematical Problems in Engineering, (2015), http://dx.doi.org/10.1155/2015/709498.
[36] S. Yadav, G. Ravichandran, Penetration resistance of laminated ceramic/polymer structures, Int J Impact Eng 28 (2003) 557-574.
[37] R. Zaera, S. Sanchez-Saez, J. L. Perez-Castellanos, C. Navarro, Modelling of the adhesive layer in mixed ceramic/metal armours subjected to impact, Composites Part A 31 (2000) 823–833.
[38] M. Grujicic, W. C. Bell, L. L. Thompson, K. L. Koudela, B. A. Cheeseman, Ballistic-protection performance of carbon-nanotube-doped poly-vinyl-ester-epoxy matrix composite armor reinforced with E-glass fiber mats, Mater Sci Eng A 479 (2008) 10–22.
[39] G.R. Johnson, T. J. Holmquist, An improved computational constitutive model for brittle materials, AIP Conf Proc 309(1994) 981-984.
[40] G.R. Johnson,W.H. Cook, A constitutive model and datafor metals subjected to large strains, high strain rates and high temperature, In: Proceedings of the 7th International Symposium on ballistics, The Hague, Netherlands 54 (1983) 1.
[41] G.R. Johnson, W.H. Cook, Fracture Characteristics of three metals subjected to various strains, strain rates, temperatures and pressures, Eng Fracture Mech 21(1985)31-48.
[42] T.Borvik, A.H. Clausen, O.S.Hopperstad, M.Langseth, Perforation of AA5083-H116 aluminium plates with conical-nose steel projectiles-experimental study, Int J Impact Eng 30(2004)367-384.
[43] S. Timoshenko, S. Woinowsky-Krieger, Theory of Plates and Shells, Mc.Graw Hill Book Company Ltd., NY, USA 2nd Edition, 1987.
[44] R.G.O'Donnell, Deformation energy of Kevlar backing plates for ceramic armours, J Mater Sci Lett 12(1993)1485-1486.
[45] Z.Rosenberg, N.S.Brar, S.J.Bless, Dynamic high pressure properties of AlN ceramics as determined by flyer plate impact, J Appl Phys 70(1991)167-171.
[46] Z. Rosenberg, Y. Yeshurn, D. G. Brandon, Dynamic response and microstructure of commercial Alumina, J Phys Colloques 46 (1985)C5-331-C5341.
[47] J. D. Clayton, Penetration resistance of armor ceramics: Dimensional analysis and property correlations, Int J Impact Eng 85 (2015) 124-131.

[48] H. Horii, S. Nemat-Nasser, Brittle fracture in compression, Splitting, Faulting and Brittle-Ductile transition, Philos Trans A 319(1986)337-374.

[49] M.F.Ashby, S. D. Hallam, The failure of brittle solids containing small cracks under compressive stress states, Acta Mater 34(1986) 497-510.

[50] J. C. LaSalvia, A physically based model for the effect of microstructure and mechanical properties on ballistic performance, in 26th Annual Conference on Composites, Advanced Ceramics, Materials, and Structures: A: Ceramic Engineering and Science Proceedings 23(2002) 213-220.

[51] K. Das, M. H. Dafadar, R. K.Varma, S. K. Biswas, Impact study of AlN-AlON ceramics, in ADVANCES IN CERAMICS ARMOR VI: Ceramic Engineering and Science Proceedings, 31 (2010) 87-95.

[52] G.Hu, K. T. Ramesh, B. Cao, J.W. McCauley, The compressive failure of aluminum nitride considered as a model advanced ceramic, J Mech Phys Solids, 59(5) (2011) 1076-1093.

[53] J. D. Clayton, A continuum description of nonlinear elasticity, slip and twinning, with application to sapphire, Proc Royal Soc Lond A 465 (2009) 307-334.

[54] H.C.Heard, C.F.Cline, Mechanical behaviour of polycrystalline BeO, Al_2O_3 and AlN at high pressure, J Mater Sci 15 (1980) 1889-1897.

[55] E.B.Zaretsky, G.I.Kenel, Evidence of ductile response of alumina ceramic under shock wave compression, Appl Pys Lett, 81 (2002) 1992.

[56] A.Seifert, A. Berger, W. F. Müller, TEM of dislocations in AIN, J Am Ceram Soc 75 (1992)873-877.

[57] M. Ueno, A. Onodera, O. Shirnomura, K. Takemura, X-ray Observation of the structural phase transition of Aluminum Nitride under high pressure, Phys Rev B 45 (1992)10123-10126.

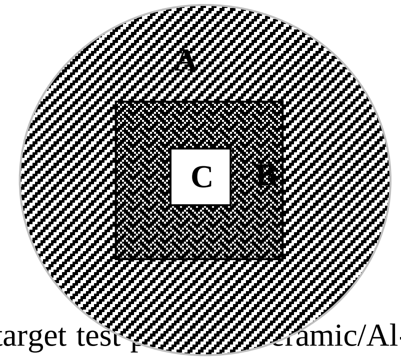

Fig. 1. Schematic drawing of target test p[illegible]eramic/Al-5083 combination, A– Al-5083 of diameter 270mm and thickness 20mm. B– GFRP frame (150mm × 150mm × 10mm) to hold the debris from flying away laterally, C– ceramic tile of dimension 50mm × 50mm × 8mm.

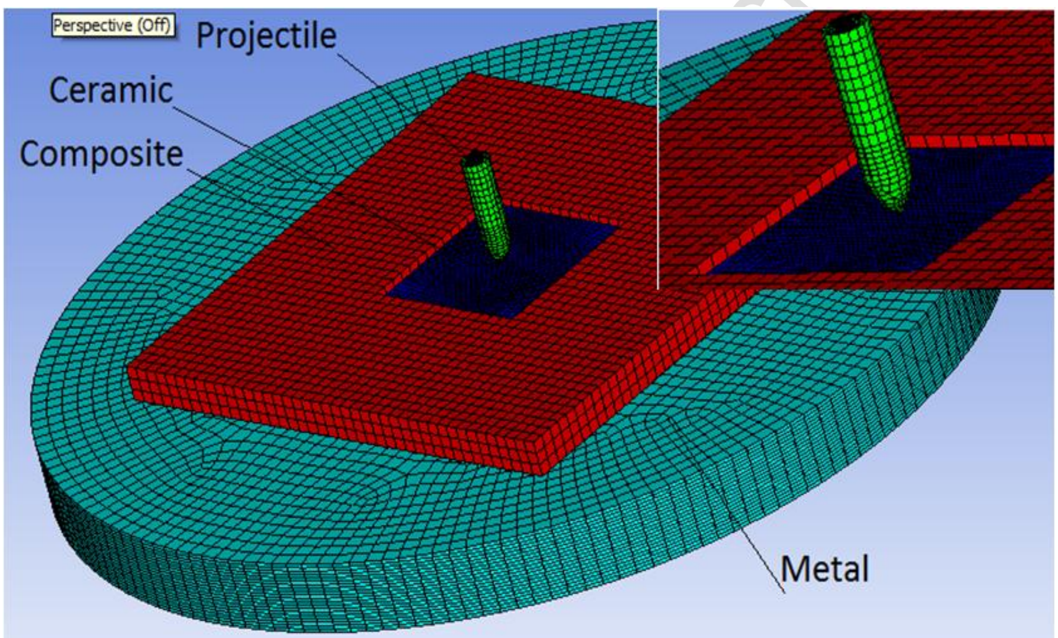

Fig. 2. Three dimensional finite element mesh model of target and projectile

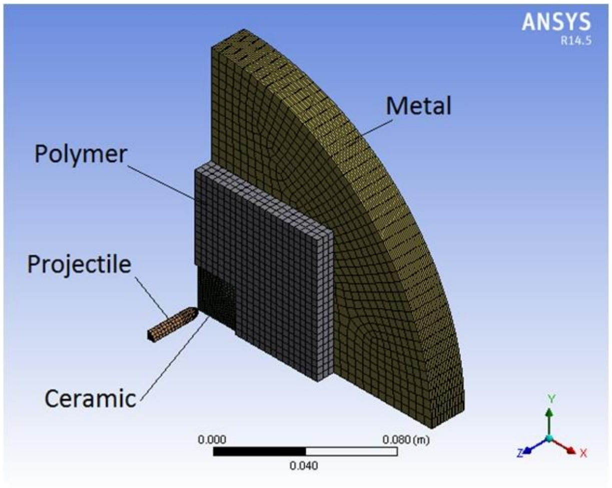

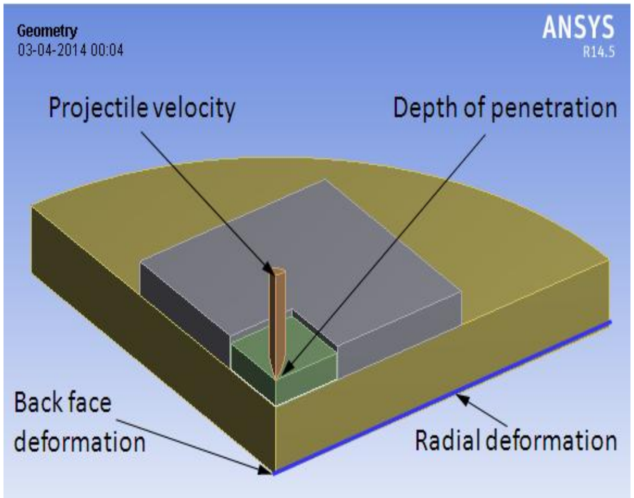

(a) (b)

Fig. 3. Quarter model of finite element geometry considered for analysis (a) quarter model with mesh (b) quarter model indicating measured parameters

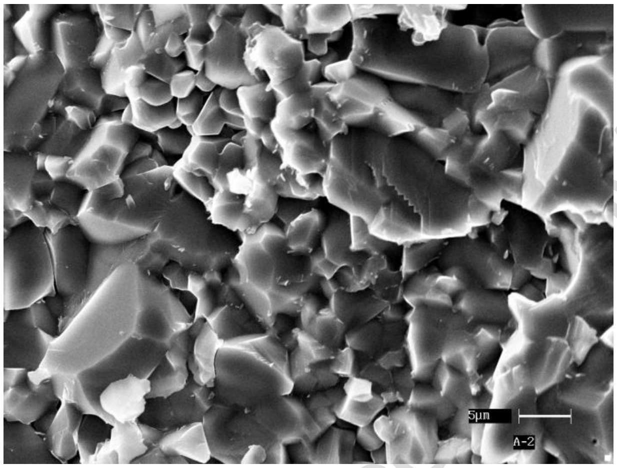

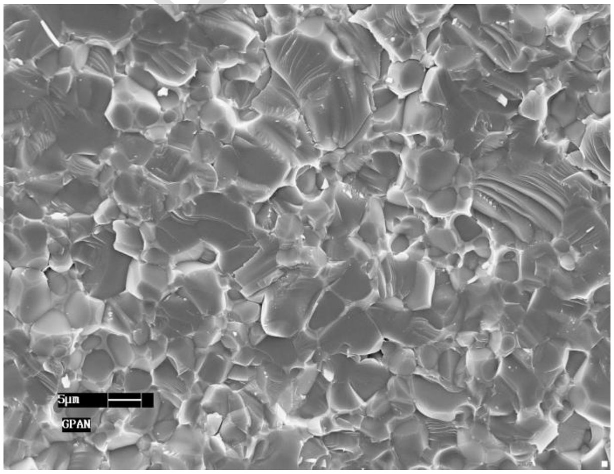

(a) (b)

Fig. 4. SEM micrograph of the fracture surfaces of (a) Al_2O_3 and (b) AlN samples.

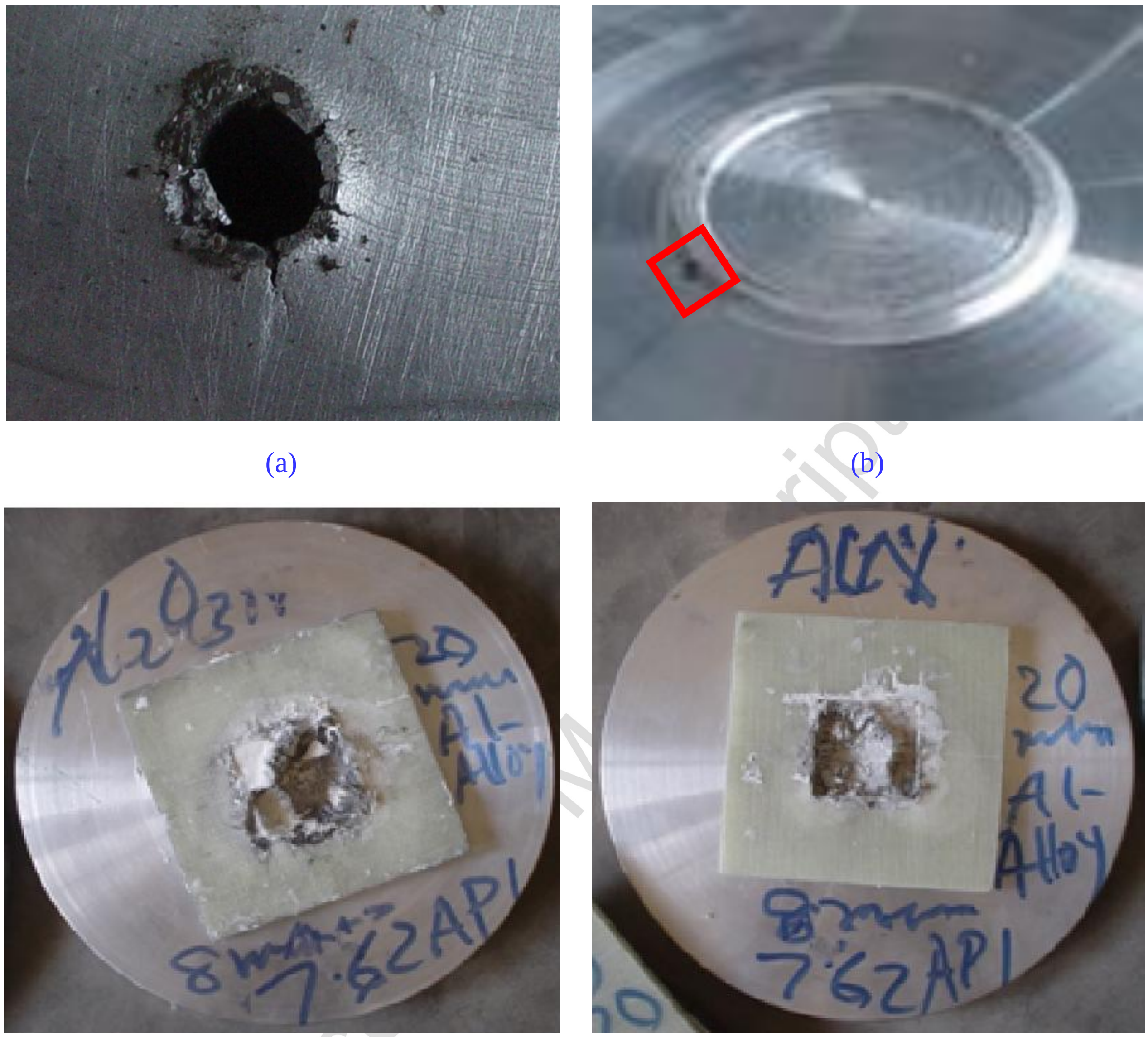

(a) (b) (c) (d)

Fig. 5. (a) Ductile hole enlargement with material accumulation (bulging) caused by the impact of 7.62AP bullets on the strike surface of Al-5083 monolithic block (125mm thickness); (b) Tip of the bullet marked by red square after machining from the opposite (back) surface of the Aluminum block to determine the depth of penetration (DOP) of the bullet and (c) Targets of Al_2O_3 /Al-5083 and (d) AlN/Al-5083 after impact by 7.62AP Bullet

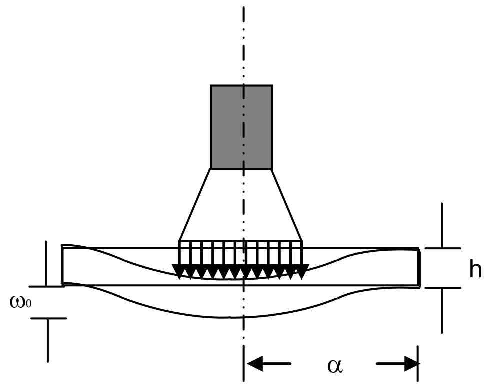

Fig. 6. Diagram of the deformation event of a circular membrane loaded at the center

Fig. 7. Bulging at the center of the Al 5083 backing plate in Al_2O_3/Al5083 armor test plate

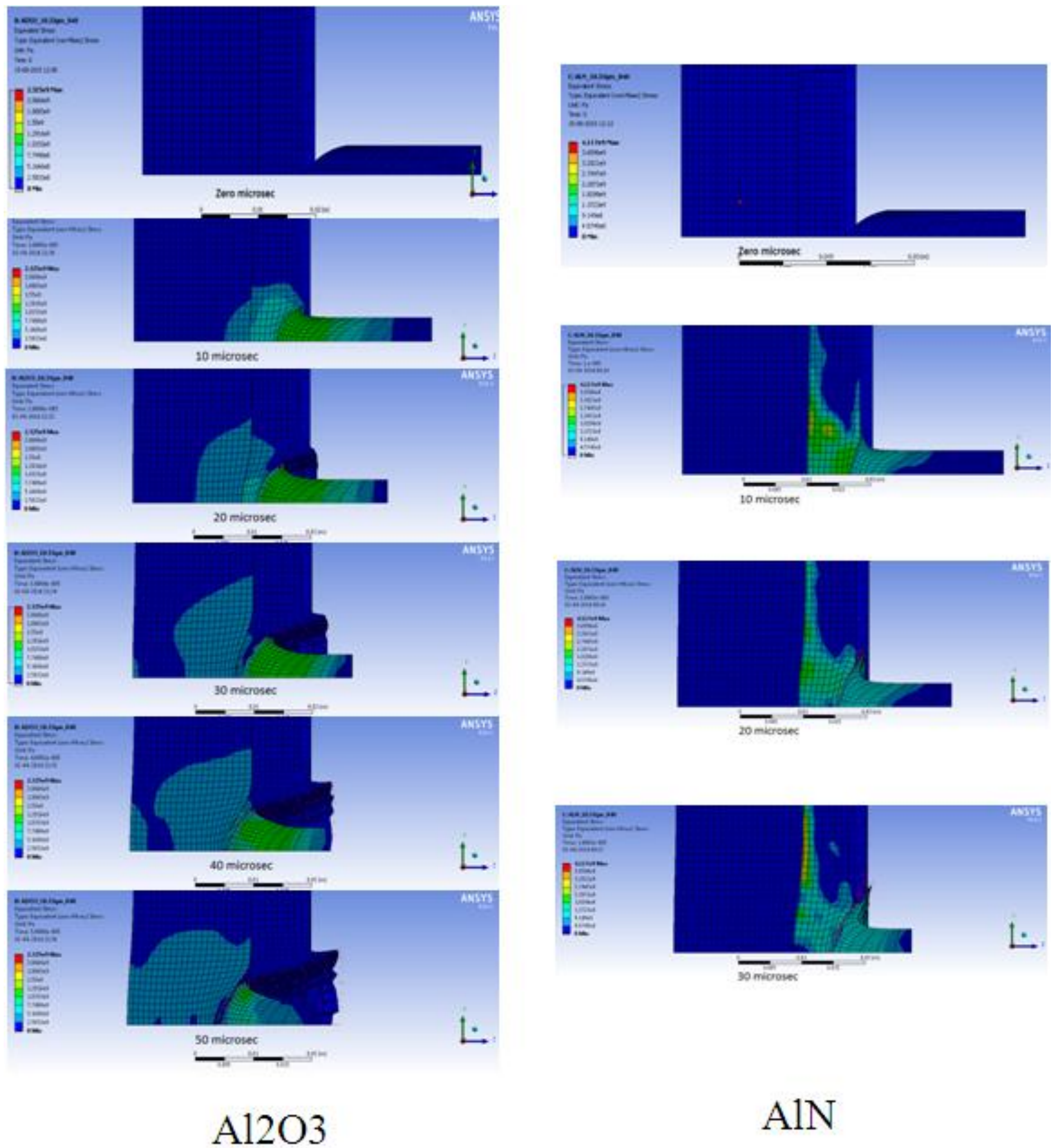

(a) (b)

Fig. 8. Comparison of projectile penetrations within (a) Al_2O_3/Al5083 and (b) AlN/Al5083 armor plate configurations with respect to time

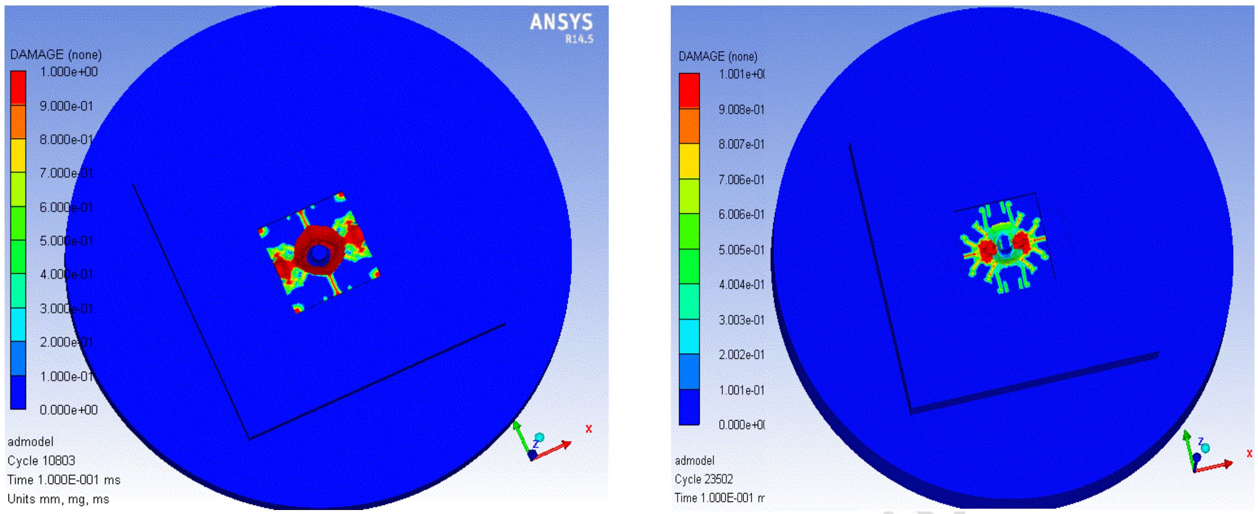

(a) (b)

Fig. 9. Damage contours on armor plate after 100 microseconds (a) Al_2O_3/Al5083 and (b)AlN/ Al5083armor plate

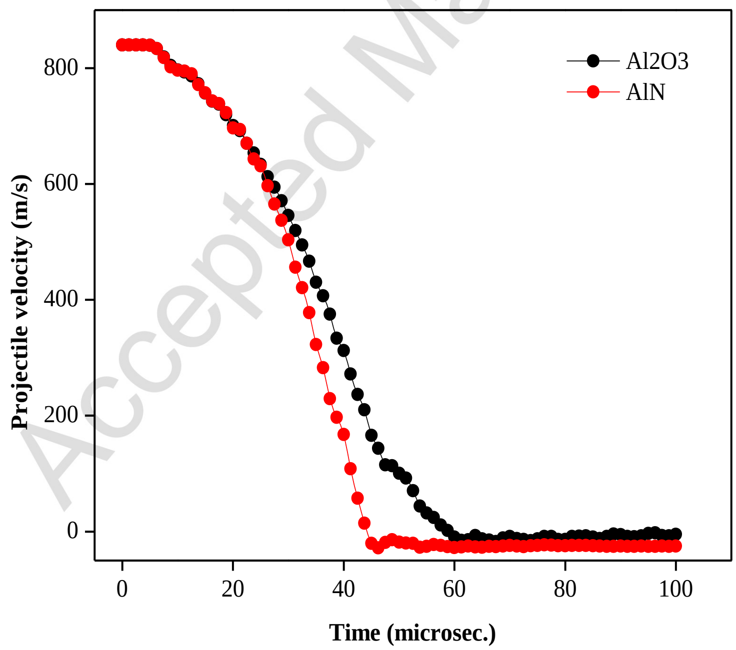

Fig. 10. Projectile velocity history with impact velocity of $840ms^{-1}$

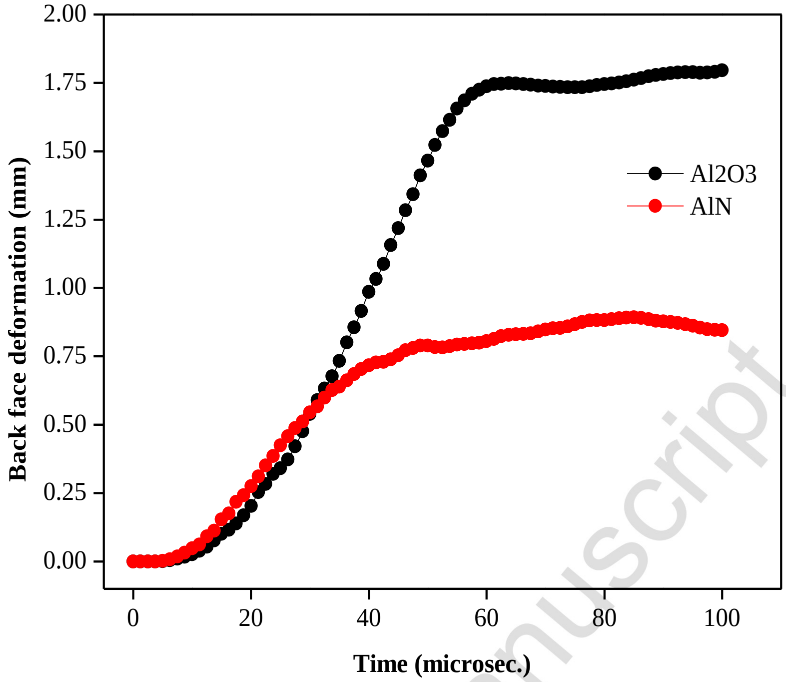

Fig. 11. Back-face deformation history at the point of impact with impact velocity of 840ms^{-1}

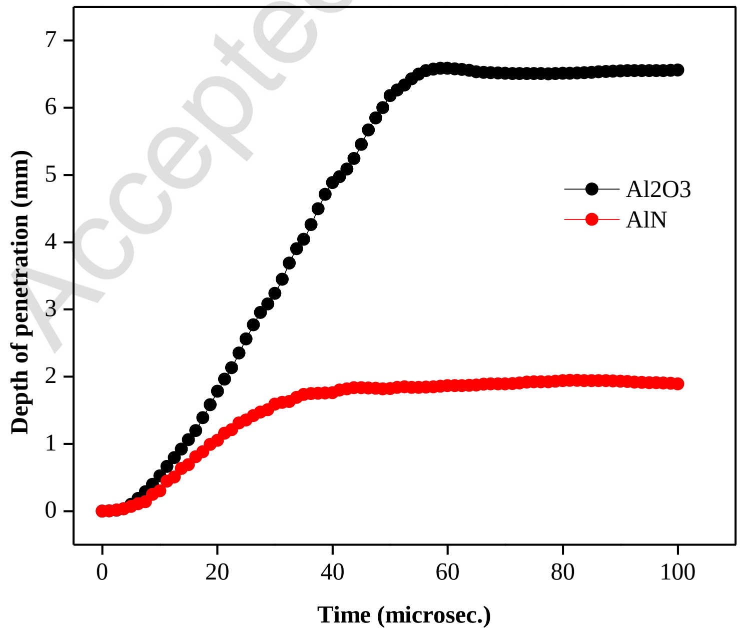

Fig. 12. History of projectiletip penetration for the two armor systems with impact velocity of 840ms^{-1}

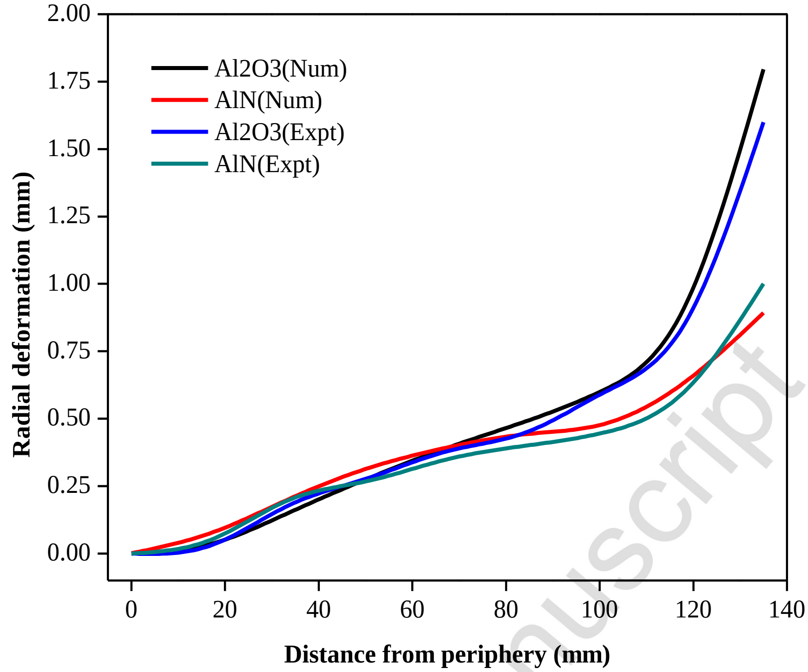

Fig. 13. Comparison of radial deformation of Al 5083 (wrought alloy) backing plates (20mm thickness) after impact in two targets having Al_2O_3 and AlN ceramics (8mm) at the front.

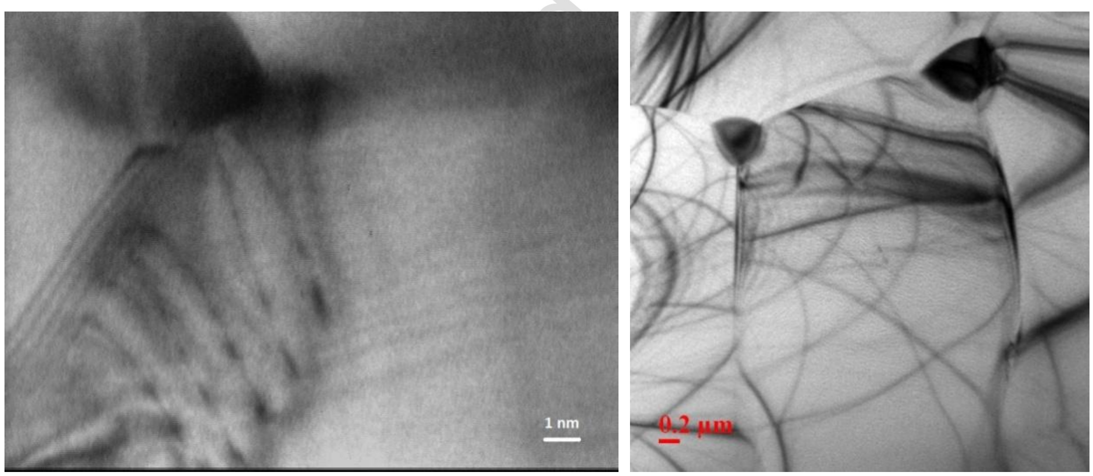

(a) (b)

Fig. 14 : TEM image of AlN specimens (a) before and (b) after the impact showing dislocations and strain contours in grains after the impact.

1 **Table 1. Specification of 7.62API Bullet (B-32, USSR).**

Length of projectile/mm	Diameter of projectile/mm	Weight of projectile/g	Muzzle Velocity/$m.s^{-1}$	Velocity at $10M/m.s^{-1}$
39	7.62	10.57	847	840

2

3 **Table 2. Properties of the Ceramic Tiles and Al-alloy (Backing Plate)**

Properties	Al_2O_3	AlN	Al-5083
Vickers' Hardness /GPa	17	10	7
Fracture Toughness (K_{IC})/$MPa.m^{1/2}$ (Indentation method)	2.5	3	---
Flexural strength/MPa (3 point bending)	233	220	---
Ultimate Tensile Strength/MPa (ASTM E8M)	---	---	272
Yield Strength/MPa (ASTM E8M)	---	---	101
Density/ $g.cm^{-3}$ (Archemedes' method)	3.82	3.33	2.72
Young's Modulus/GPa(Ultrasonic velocity measurement)	366	331	72
Shear Modulus (Ultrasonic velocity measurement)	147	133	---

4
5
6
7
8
9
10 **Table 3.** Material models used in simulation

Descriptor	Equation of state	Strength	Failure
Al_2O_3/AlN	Polynomial	Johnson Holmquist-2	Johnson Holmquist-2

PolyuretheneResin	Shock	--	--
Steel 4340	Linear	Johnson Cook	Johnson Cook
Al5083	Linear	Johnson Cook	Hydro (P_{min})

Table 4. Experimental values for Depth of Penetration (DOP) and Back Face Deformation (BFD)

Configuration (thickness/mm)	**Depth of Penetration (/mm)**			**Back-Face Deformation (/mm)**		
	Expt.1	Expt.2	Expt.3	Expt.1	Expt.2	Expt.3
Al5083 (125)	62.5	65	60	-	-	-
Al_2O_3(8)/Al5083 (20)	6	6.8	6.4	1.4	1.6	1.5
AlN(8)/Al5083(20)	3	2.5	2	1.2	1	0.8